Journal of The Electrochemical Society

The Electrochemical Society
Advancing solid state & electrochemical science & technology

OPEN ACCESS

Impact of the Anode Catalyst Layer Design on the Performance of H_2O_2-Direct Borohydride Fuel Cells

Impact of the Anode Catalyst Layer Design on the Performance of H_2O_2-Direct Borohydride Fuel Cells

Rachel M. E. Hjelm,[1] Clémence Lafforgue,[2] Robert W. Atkinson III,[3] Yannick Garsany,[4] Richard O. Stroman,[5] Marian Chatenet,[2,*] and Karen Swider-Lyons[5,*,z]

[1] *NRC Research Associate Program, Assigned to NRL*
[2] *Univ. Grenoble Alpes, Univ. Savoie Mont Blanc, CNRS, Grenoble INP, LEPMI, 38000 Grenoble, France*
[3] *ASEE Research Associate Program, Assigned NRL*
[4] *Excet Inc, Springfield, Virginia, USA*
[5] *United States Naval Research Laboratory, Washington, DC, USA*

Pt and Pd electrocatalysts are active for the complex 8-electron borohydride oxidation reaction (BOR), but the completeness of the electrochemical reaction is compromised by the formation of byproducts, including unreacted H_2. We probe how combining the two electrocatalysts might improve the overall BOR activity. Five catalyst layer compositions are compared by rotating disk electrode (RDE) voltammetry and as the anode in hydrogen-peroxide direct borohydride fuel cells (H_2O_2-DBFCs): Pt/C, Pd/C, a Pt/C + Pd/C mixture, and graded layers of Pt/C and Pd/C as Pt/C|Pd/C or Pd/C|Pt/C. The RDE results show distinct mechanistic pathways for Pt and Pd, electrodes, but that the mixtures and Pt/C|Pd/C graded electrodes lead to better BOR activity than Pt or Pd alone. Similarly, the graded anodes in H_2O_2-DBFC outperform the ones with pure Pt/C or Pd/C under several operational conditions due to synergy between Pt and Pd. The Pt and Pd appear to serve as cooperative electrocatalysts, with their combination leading to less deleterious H_2 escape than cells with Pt-only electrodes, and higher electrochemical performance than cells with Pd-only electrodes. We conclude that catalyst layers with graded compositions are promising electrode architectures for DBFCs.
 [DOI: 10.1149/2.0681914jes]

Manuscript submitted April 19, 2019; revised manuscript received August 9, 2019. Published November 15, 2019. This was Paper 1614 presented at the National Harbor, Maryland Meeting of the Society, October 1–5, 2017.

We attempt to improve the efficacy of a hydrogen peroxide/direct borohydride fuel cell (H_2O_2-DBFC) by grading and mixing Pt/C and Pd/C electrocatalysts and improve the overall borohydride oxidation reaction (BOR). The oxidation of BH_4^- to BO_2^- releases up to eight electrons making it an energy-dense reaction. The half-cell reaction for the H_2O_2-DBFC is in Eq. 1 with the electrochemical potential expressed on the standard hydrogen electrode (SHE) scale.

$$BH_4^-(aq) + 8\,OH^- \leftrightharpoons BO_2^-(aq) + 6\,H_2O + 8\,e^- \qquad E^o_{BOR} = -1.24\ V\ vs.\ SHE \qquad [1]$$

The hydrogen peroxide reduction reaction (HPRR) at the cathode gives a theoretical half-cell potential of 1.76 V vs. SHE (Eq. 2). Combining Equations 1 and 2 suggests that the theoretical cell voltage (U_{Cell}) of a H_2O_2-DBFC is 3.01 V (Eq. 3). The practical cell voltage is $U_{Cell} = 3.01 - 0.83\ V = 2.18\ V$ when accounting for the unavoidable junction potential between the high pH fuel solution and low pH oxidizer solution.[1]

$$H_2O_2 + 2\,H^+ + 2\,e^- \leftrightharpoons 2\,H_2O \qquad E^o_{HPRR} = 1.76\ V\ vs.\ SHE \qquad [2]$$

$$BH_4^-(aq) + 8\,OH^- + 4\,H_2O_2 + 8\,H^+ \leftrightharpoons BO_2^-(aq) + 14\,H_2O \qquad U_{cell} = 3.01\ V \qquad [3]$$

The path to the 8-electron electrooxidation process from BH_4^- to BO_2^-, produces a number of reaction intermediates ($BH_{x,ads}$ or BH_xOH^-, $x = 1$ to 3), which change with the nature and structure of the electrocatalyst, the electrode architecture, the cell temperature, the pH, and the concentration of the $NaBH_4$ in the alkaline fuel.[2,3] Unwanted byproducts include molecular hydrogen that adsorbs on the electroactive surfaces (H_{ads}), and hydrogen gas (H_2). H_2 production is the result of two possible processes. One is the electrocatalytic reduction of water (hydrogen evolution reaction, HER), which occurs below the hydrogen potential.[4] The other is the non-electrochemical heterogeneous hydrolysis or catalytic decomposition of BH_4^- to BO_2^- (Eq. 4) and/or of some reaction intermediates (e.g., $BH_{x,ads}$ or BH_xOH^-). Both processes often occur as parasitic reactions in parallel with BH_4^- electrooxidation, and possibly both below (HER and hydrolysis) and above (hydrolysis) the hydrogen potential.[3–5] Ideally, the H_2 is electrooxidized by the electrocatalyst (Eq. 5) to generate more power, rather than being lost via escape.[6] H_2 gas bubbles may also physically block access to catalyst active surfaces by blocking the electrode structure. All of this complexity leads to varied reaction species concentrations along the fuel cell flow channel.[7]

$$BH_4^-(aq) + 2\,H_2O \rightarrow BO_2^-(aq) + 4\,H_2 \qquad [4]$$

$$H_2 + 2\,OH^- \leftrightharpoons 2\,H_2O + 2\,e^- \qquad E^o_{HOR} = -0.828\ V\ vs.\ SHE \qquad [5]$$

Numerous electrocatalysts have been studied for the BOR (e.g., Pt, Pd, Au, Ni, their alloys as well as AB_5 and AB_2-type hydrogen storage alloys).[8] However, no single anode electrocatalyst has been fully effective in practical DBFCs. Pt has significant activity for the BOR as well as for H_2 and H_{ads} oxidation,[3,5] making it attractive in high-power-density DBFC applications.[9] Pt also favors the non-electrochemical heterogeneous hydrolysis of BH_4^-, which lowers the available BH_4^- for electrooxidation and increases H_2 production.[4] The Pt activity is lowered from poisoning by BH_{ads} intermediate species at low potentials, and oxide species when polarized above 0.50 V vs the reversible hydrogen electrode (RHE),[3,10] resulting in high levels of H_2 production.

The drawbacks of Pt electrocatalysts might be alleviated by combining them with a Pd electrocatalyst. Pd has been studied for the BOR as a single electrocatalyst,[2,11–14] or as an alloy with varied metals.[11,15,16] Pd is electrocatalytically-active for both the oxidation of BH_4^- and of its intermediates, as well as for H_2 generation/oxidation; however the reaction kinetics are slower than for Pt.[9] Pd is also susceptible to poisoning by $BH_{ads,}$ although in a lesser extent than Pt.[10] The role of Pd as a cooperative catalyst (or co-catalyst) was shown by Oliveira et al.[17,18] who found that the addition of a monolayer of Pd to Pt (111) enhances the BOR activity of Pt in half-cell measurements (for dilute $NaBH_4$ electrolytes: $[NaBH_4] = 1$ mM). The improvements in performance of the Pt(111)-supported Pd adlayers were attributed to the increase in partial dissociation of BH_4^- to BH_3 species by Pd, where the $BH_{3,ads}$ species produced is more easily electrooxidized by Pt (and Pd) than the BH_{ads} species that spontaneously form on Pt.[5,10]

We hypothesize that combining high surface area Pt and Pd electrocatalysts will improve the BOR activity and efficiency, with the thesis that each electrocatalyst is more effective at different aspects

*Electrochemical Society Member.
ᶻE-mail: karen.lyons@nrl.navy.mil

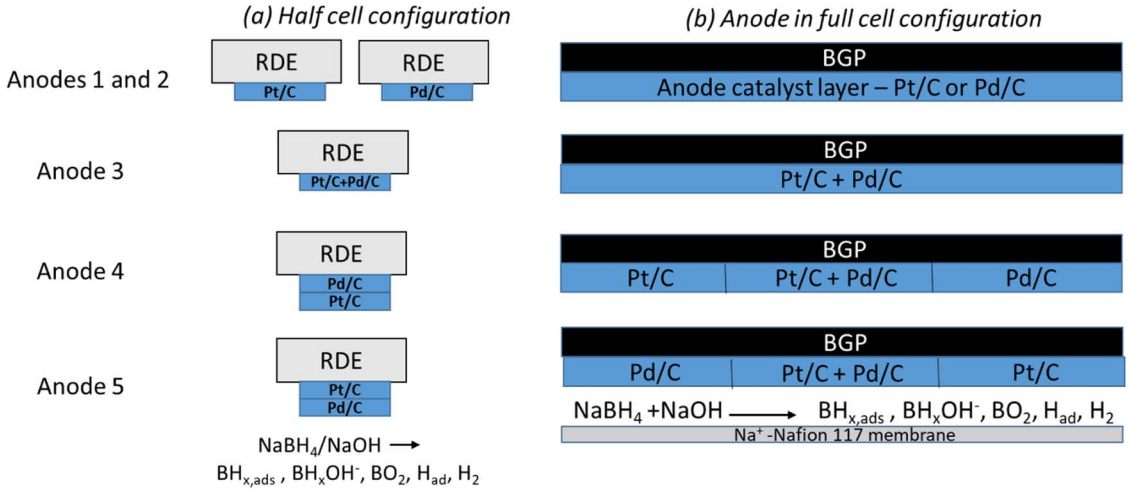

Figure 1. Schematics of the five anode catalyst layer designs (a) on rotating disk electrodes (RDEs) and (b) on the graphitic bipolar plates (GBPs) in H_2O_2 -DBFCs. See the text and Figure 2 for accurate dimensions.

of the BOR, so each might favor the steps in the BOR better than the other and they might serve as cooperative electrocatalysts. With Pd at the inlet, one might expect a more complete BH_4^- oxidation, with any excess H_2 easily electrochemically oxidized by Pt at the outlet. Pt at the inlet might promote higher initial activity to the BOR but be poisoned, leaving Pd at the outlet to react the remaining, diluted borohydride intermediates. We also look at mixtures as a standard variation to determine whether the combination of catalysts is important in a specific order, or in a sequential sequence. We have previously shown preliminary results on this concept,[19] and now report the results in greater depth.

The BOR individual electrocatalysts, simple mixtures and graded mixtures are studied by rotating disk electrode (RDE) voltammetry with the electrode configurations shown in Figure 1a in a solution with 0.01 M $NaBH_4$ fuel in 1 M NaOH electrolyte. The electrocatalysts are examined in a full H_2O_2-DBFC with the five different anode configurations in Figure 1b: Pt/C, Pd/C, a 1:1 wt% Pt/C and Pd/C mixture, Pt/C graded to Pd/C (Pt/C|Pd/C), and Pd/C graded to Pt/C (Pd/C|Pt/C). The electrocatalysts are deposited onto graphite bipolar plates (GBPs) via ultrasonic spray. The cell design is based on a well-characterized single-flow-channel H_2O_2-DBFC (see Figure 2),[7,19] and the anode fuel is either 0.01 or 0.10 M $NaBH_4$ in 1 M NaOH. The cathodes for the H_2O_2-DBFCs comprise high surface area Pt/C on GBPs in an oxidizer solution of either 0.04 or 0.40 M H_2O_2 in 1 M H_2SO_4. The process of H_2O_2 reduction at the Pt/C cathode is less complex than that of BOR and the reaction rates are faster,[20,21] so any differences in electrochemical behavior and performance of each H_2O_2-DBFCs should be attributed to change in performance of the anode catalyst. The anode and cathode compartments are separated from the anode by the Na^+ form of a perfluorosulfonic acid membrane. *H_2 escape* and

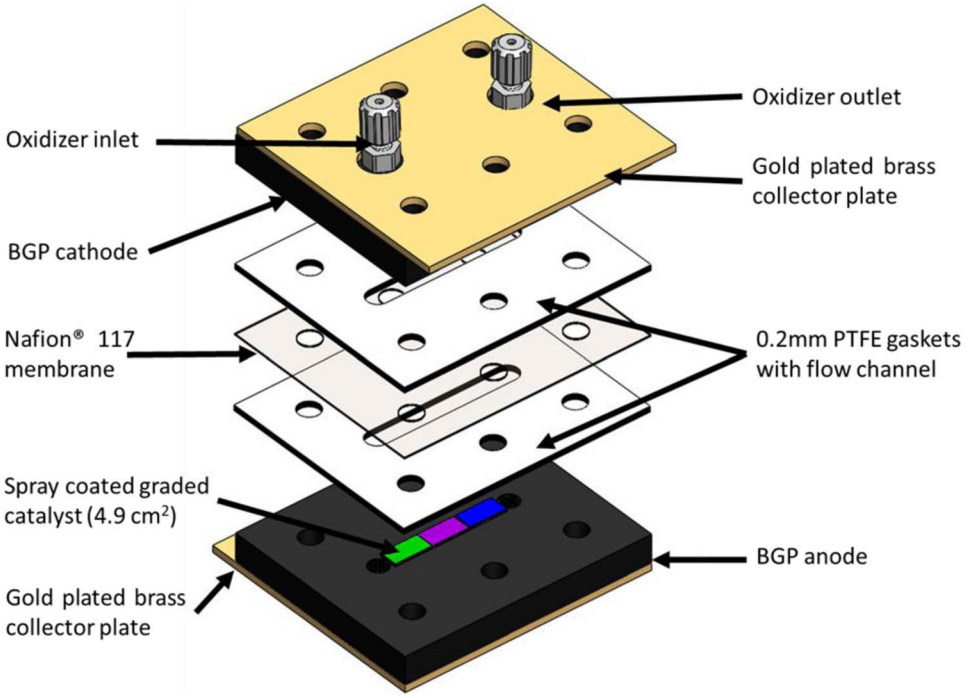

Figure 2. 3D exploded view of the H_2O_2-DBFC cell showing a graded anode catalyst with Pt/C (green), 1:1 wt % Pt/C + Pd/C (purple), and Pd/C (blue). The fuel inlet and outlet are hidden, but mirror the oxidizer inlet and outlet at the top. The gaskets create flow field that are approximately 0.2 mm deep.

electrochemical impedance spectroscopy (EIS) provide additional insights into the different current and reaction mechanisms of each anode.

Experimental

Electrocatalysts.—*Pt/C electrocatalysts.*—A 20 wt% Pt/Vulcan XC72 (2 nm Pt particle size) was purchased from Tanaka Kikinzoku and used as received without any treatment for RDE experiments. A 50 wt% Pt/C (2.5 nm Pt particle size) was purchased from Ion Power and used as received for the H_2O_2-DBFC experiments.

Pd/C synthesis and characterization.—The Pd/C electrocatalysts were prepared by vapor deposition of Pd onto Vulcan carbon support.[22–24] The Vulcan carbon support (XC-72, Cabot) and powdered precursor (palladium II (2,4)-pentanedionate; 99%, Sigma Aldrich) were combined and mixed in a borosilicate vial. Support and precursor masses were chosen to produce 250 mg total of the carbon-supported Pd electrocatalyst in a range of targeted metal weight fraction of 20 and 50 wt% Pd. The vials were then transferred to a vacuum oven. After the oven was sealed, air was evacuated and replaced by dry nitrogen. The oven was heated to 170°C at 0.752 atm and allowed to dwell for 15 h. At this temperature and pressure, the precursor sublimed, reacted with the carbon support surfaces, and Pd nanoparticles were grown on the Vulcan carbon support. The oven was then cooled passively to room temperature before the catalyst powders were removed. The sample masses were recorded to determine final weight fractions of Pd/C and found to be 22 and 53 wt % Pd. Samples were heat-treated at 180°C for 2 h in a flowing 10% H_2 (balance Argon) mixture to remove interstitial carbon that was absorbed into the palladium lattice during synthesis from decomposition of the organic ligands in the Pd precursor.[25,26]

ECSAs.—The electrochemical surface areas (ECSAs) of the electrocatalysts were measured using CO_{ads}-stripping coulometry assuming that the electrooxidation of one monolayer of CO_{ads} requires 420 $\mu C\ cm_{metal}{}^{-2}$. The Pt ECSAs are 78 and 86 $m^2\ g_{Pt}{}^{-1}$ for the 20 wt% Pt/C and 50 wt% Pt/C, respectively. The Pd ECSAs are 23 and 64 $m^2\ g_{Pd}{}^{-1}$ for the 22 wt% Pd/C and 53 wt% Pd/C, respectively. The 22 wt% Pd/C was used for RDE experiments and the 53 wt% Pd/C was used for H_2O_2-DBFC experiments.

RDE characterization.—Thin-film RDE experiments were conducted using a four-electrode electrochemical cell with a measured temperature $T = 25$°C connected to a BioLogic potentiostat (VMP3). The counter electrode was a glassy-carbon plate and the reference electrode was a commercial Hg/HgO electrode filled with 1 M NaOH and connected to the cell via a Luggin capillary, but all the potentials are expressed on the RHE scale. A gold wire connected to the reference electrode was used to filter the high frequency electrical noise.[27] The bottom of the cell was made of Poly chloro trifluoro ethylene (PCTFE) in order to avoid glass contact with concentrated alkaline solution. All the glassware and plastic accessories used for the experiments were soaked in Caro's acid (1:1 vol. % H_2O_2 (30%)-H_2SO_4 (>95 wt%)) overnight, in order to prevent any metallic and organic pollution, and thoroughly rinsed with ultrapure water (18.2 MΩ cm, <3 ppb Total Organic Carbon, Millipore Elix + Gradient, Millipore) prior to each experiment. The electrolyte (0.01 M $NaBH_4$ in 1 M NaOH) was prepared daily using $NaBH_4$ powder (>98 %, Merck) and NaOH, H_2O crystals (Suprapur, Merck) dissolved in ultrapure water.

The working electrodes were prepared using suspensions made of electrocatalyst, ultrapure water, 5 wt% Nafion solution and isopropyl alcohol (IPA) in quantities given in Table I. After 20 min of sonication, the Pd/C, Pt/C and mixed electrodes were prepared by depositing, respectively, 20 µL of ink #1, ink #2, and ink #3 on a 5 mm-diameter glassy carbon electrode (i.e. geometric surface area = 0.196 cm^2) that was rotated throughout film drying to achieve a uniform film thickness, as recommended by Garsany et al.[28] The graded Pt/C|Pd/C and Pd/C|Pt/C electrodes were prepared by first depositing 10 µL of ink #1 (respectively ink #2) and then rotating it until dry. Subsequently, a second film was formed by deposition of 10 µL of ink #2 (respectively ink #1) and then dried under rotation. This approach gives a graded porous thin-film, in which the Pt/C layer is at the outer surface, i.e. in direct contact with the electrolyte, or, in which the Pd/C layer is at the outer surface, i.e. in direct contact with the electrolyte, as illustrated in Fig. 1.

The electrochemical measurements consisted of first recording three cyclic voltammograms (CVs) in the supporting electrolyte (1 M NaOH) from an electrode potential $E = 0.01$ to 1.50 V vs RHE at a potential sweep rate (v) of 100 mV s^{-1} and three more CVs at $v = 20$ mV s^{-1}. Then, $NaBH_4$ was added to the supporting electrolyte and the electrooxidation of $BH_4{}^-$ was studied by recording one CV from E = -0.10 V to 1.50 V vs. RHE at $v = 20$ mV s^{-1}, this CV being repeated for different rotation rates (ω) of the RDE in the following order: 400, 900, 1600, 2500, 0 and 400 revolution per minute (rpm). Three different tests were carried out for each electrode configuration and the error bars were calculated using the standard deviation.

Fuel cell development and characterization.—*Cell design.*—Figure 2 shows an exploded 3D view of the components of the H_2O_2-DBFC. Each cell consisted of a Nafion 117 membrane (183-µm thick), two PTFE gaskets (200-µm thick) each with a 0.48 cm × 5.08 cm (2.45 cm^2) flow channel cut in the center, and impervious BGPs (Fuel Cell Store) at both the anode and cathode. Catalyst layers were coated on one side of the BGP, and in contact with brass current collector plates on the other side. According to the vendor, the impervious BGPs have high electrical and thermal conductivity, high resistance to chemicals, and are densified and resin-filled for low electrolyte permeability. The cells leaked significantly if fuel-cell-grade graphitic bipolar plates were used, making the impervious BGPs compulsory. The flow inlet and outlet were at the ends of each catalyst layer. The Nafion 117 membranes were converted to their Na^+ form by first cleaning the membranes in a boiling solution of 1 wt% H_2O_2 for 1 hour followed by boiling the membranes in 0.10 M NaOH for 1 hour. Membranes were stored in the 0.1 M NaOH solution until use.

Ultrasonic spray-coating of catalysts layers.—Inks for the anode catalyst layers were made from the 53 wt % Pd/C and the commercial 50 wt % Pt/C using the procedure described by Sassin et al.[29] Inks for the cathode were made from the commercial 50 wt % Pt/C. All inks were prepared using 6 wt % Aquivion 830 EW ionomer (D83-06A, Sigma Aldrich). The mass ratio of the ionomer to carbon (I/C) was adjusted to 0.95 (i.e. 32 wt % ionomer in the dry catalyst layer). For some experiments, a 1:1 wt % mixture of Pt/C and Pd/C was combined using the same weight for each electrocatalyst and the same I/C as the homogeneous inks.

Table I. Ink compositions and metal loading for the RDEs.

	20 wt% Pt/C (TKK) (mg)	22 wt% Pd/C (NRL) (mg)	H_2O (µL)	Nafion (µL)	IPA (µL)	Metal Loading ($\mu g_{metal}\ cm^{-2}{}_{geom}$)
Ink #1	0	10	8000	53.5	3150	20
Ink #2	10	0	7130	55	3000	20
Ink #3	5	5	7130	55	3000	20

Table II. Compositions of the five H_2O_2-DBFCs anode catalyst layers.

		Electrocatalyst	Noble metal loading (mg_{metal} cm^{-2})
Pt/C H_2O_2-DBFC	Anode	50 wt% Pt/C	0.31± 0.02
	Cathode	50 wt% Pt/C	0.31 ± 0.02
Pd/C H_2O_2-DBFC	Anode	53 wt% Pd/C	0.30 ± 0.01
	Cathode	50 wt% Pt/C	0.31 ± 0.02
Mixed Pt/C+ Pd/C H_2O_2-DBFC	Anode	50 wt% Pt/C + 53 wt% Pd/C	0.30 ± 0.02
	Cathode	50 wt% Pt/C	0.31 ± 0.02
Graded Pt/C|Pd/C and Pd/C|Pt/C H_2O_2-DBFC	Anode	50 wt% Pt/C|50 wt% Pt/C + 53 wt% Pd/C|Pd/C	0.31 ± 0.01
	Cathode	50 wt% Pt/C	0.31 ± 0.02

Pt/C and Pd/C inks were ultrasonically spray-coated onto the impervious BGPs using the method also described in reference 29. The catalyst area for each electrode was a 0.965 cm × 5.08 cm (4.9 cm^2 0.96 cm × 5.08 cm (4.90cm^2)) rectangle spanning from inlet to outlet. For the anodes, Pt/C and Pd/C were sprayed as individual electrodes, in 1:1 wt% mixtures Pt/C + Pd/C, and as gradients. For single and mixed electrodes, inks were deposited uniformly along the entirety of the flow field area. For anodes with graded catalyst layers, masks were made to spray 1/3 of the area at a time such that Pt/C and Pd/C were deposited at each end of the flow field with a Pt/C+Pd/C mixture at the center, creating a gradual transition from Pt/C to Pd/C or Pd/C to Pt/C (see Fig. 1). Each sprayed electrode was dried overnight before testing to ensure complete evaporation of the solvent. Catalyst layers were similarly deposited as dummy electrodes onto Kapton foil and weighed 5 times after overnight drying. The average of the resulting weights for the Pt, Pd, and mixed samples were 0.31 ± 0.02 mg cm^{-2}, 0.30 ± 0.01 mg cm^{-2}, and 0.30 ± 0.02 mg cm^{-2}, respectively. Table II summarizes the electrocatalysts for the five different H_2O_2-DBFC configurations.

Cell operation and electrochemical evaluation.—Two different combinations of fuel and oxidizer were used:

1. 0.01 M $NaBH_4$ in 1 M NaOH electrolyte at the anode and 0.04 M H_2O_2 in 1 M H_2SO_4 electrolyte at the cathode.
2. 0.10 M $NaBH_4$ in 1 M NaOH electrolyte at the anode and 0.40 M H_2O_2 in 1 M H_2SO_4 electrolyte at the cathode.

Solutions of 1 M H_2SO_4 (98%, Fisher Scientific) and 1 M NaOH (pellets, Fisher Scientific) were prepared and then cooled to room temperature. $NaBH_4$ (98% granules, Alfa Aesar) and H_2O_2 (30%, Fisher Scientific) were added to the 1 M NaOH or 1 M H_2SO_4 solutions, respectively, within 30 minutes of use to minimize the amount of fuel or oxidizer degradation prior to testing.

Each H_2O_2-DBFC was evaluated electrochemically using an Autolab potentiostat/galvanostat with an impedance analysis module (FRA2) coupled with an Autolab Eco Chemie 10A Current Booster and NOVA 2.1 software to measure polarization curves and EIS. A flow rate of 10 mL min^{-1} was maintained at both the cathode and anode with parallel flow using two peristaltic pumps (NE-9000, Chemyx). All cells were operated at room temperature (25°C). The open circuit voltage (OCV) of each cell was measured for 5 min prior to measuring each polarization curve. Cell voltages (U_{Cell} / V) were held for 150 s starting at OCV and measured every 100 mV vs. OCV until polarized to 1.40 V. The current at each cell voltage was measured every second and the last 20 points were averaged. Current was normalized to the active geometric area of the flow field (i.e. 2.45 cm^2) to give geometric current density (j_{geom} / mA cm^{-2}). A total of three of each H_2O_2-DBFC anode configuration was measured. Polarization curves were plotted as cell voltage vs geometric current density and power curves were plotted as power density (P_{geom} / mW cm^{-2}) vs. geometric current density.

Escaped gaseous H_2 was measured in mL concurrently with the polarization curves measurements using an inverted graduated cylinder connected to the flow channel outlet at the anode. The measured volumes were divided by the time of each current measurement to give the rate of H_2 *escape* (μL s^{-1}) and plotted as H_2 *escape* vs. geometric current density.

Percent fuel utilization (η / %) was calculated using Eq. 6,

$$\eta = \frac{I}{\left[BH_4^-\right] * VFR * F * 8} * 100 \quad [6]$$

where I is the current measured (A), $[BH_4^-]$ is the concentration of BH_4^- (mol cm^{-3}) feeding into the cell at the volumetric flow rate (VFR, cm^3 s^{-1}), F is the Faraday constant (A s mol^{-1}) and 8 is the theoretical (maximal) number of electrons produced per BH_4^- species. Given a flow rate of 10 mL min^{-1} (0.167 cm^3 s^{-1}), the theoretical currents for 0.01 and 0.10 M $NaBH_4$ were calculated as 1.29 A (j_{geom} = 0.53 A cm^{-2}) and 12.9 A (j_{geom} = 5.30 A cm^{-2}), respectively. These theoretical values assume that each BH_4^- anion was completely oxidized to BO_2^- in an 8-electron reaction without H_2 generation (and that the H_2O_2 cathode is not limiting the cell operation).

The EIS was measured at cell voltages of 1.45 V and 0.85 V in a frequency (ν) range between 10 kHz to 0.1 Hz with 10 measurements per decade, with RMS_{max} set to 0.10 V. The relatively high RMS_{max} was used to reduce noise at low frequency impedance. The results were normalized to the geometric area of the active flow field and were plotted as the real (Z' / Ω cm^2) vs. imaginary impedance (−Z'' / Ω cm^2).

Results

Rotating disk electrode configuration measurements.—The BOR activities are shown in Figure 3 for the five electrode structures in Fig. 1a as measured by RDE voltammetry. The current densities presented in the CVs were obtained by dividing the measured current either by the corresponding ECSA (cm^2) of each electrocatalyst (see Fig. 3a) in the case of the mixed and graded electrodes, the ECSA used to calculate the current densities is the average between the Pt/C ECSA and Pd/C ECSA) or by the electrode's geometric surface area (see Fig. 3b).

The overall CV shapes are different for the Pt/C-only and the Pd/C-only electrodes while the CVs obtained with the other three electrode configurations (mixed Pt/C + Pd/C or graded electrodes) are all similar to the Pt-only electrode. In addition, the open-circuit potentials (OCPs, corresponding to E (I = 0 A)) reached on all the Pt-containing electrodes are around −45 mV vs. RHE whereas it is −114 mV vs. RHE for the Pd/C-only electrode (see Fig. 4a). These results suggest that the mixed and graded electrode structures may lead to a similar BOR mechanism than the Pt/C-only electrode, and that in consequence, the behavior of Pt/C dominates in these cases. For all the Pt-containing electrodes, the HER prevails on the BOR below E = 0 V vs. RHE; above this potential, the HOR prevails on the BOR. This is because Pt tends to decompose BH_4^- into $BH_{x,ads}$ + H_{ads} (H_{ads} likely combining into H_2 below the hydrogen potential and being oxidized above this potential) and because Pt is highly active for the HER/HOR. We conclude that the OCP is dominated by the HER/HOR on Pt and is not affected by the addition of Pd in the mixed and graded electrodes.

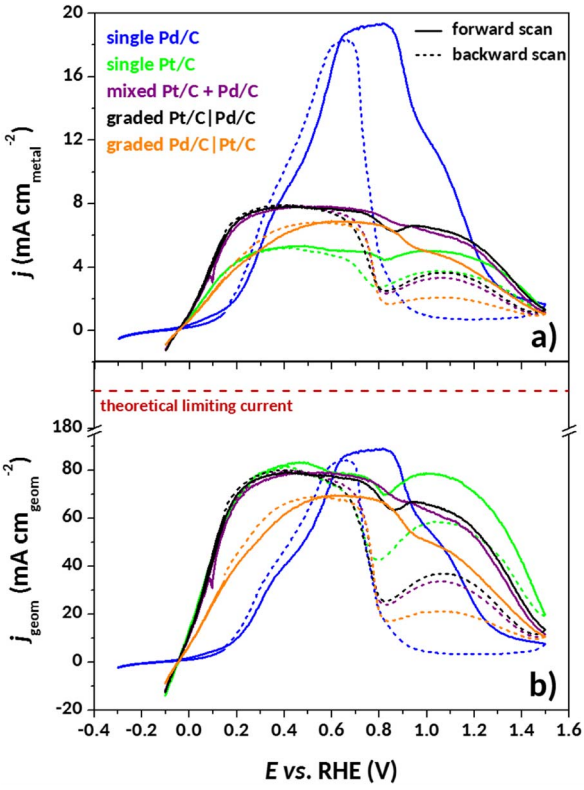

Figure 3. BOR voltammograms recorded on Pd/C (blue), Pt/C (green), mixed Pt/C + Pd/C (purple), graded Pt/C|Pd/C (black), and graded Pd/C|Pt/C (orange) working electrodes, in 0.01 M $NaBH_4$ + 1 M NaOH, $\nu = 20$ mV s^{-1}, $\omega = 1600$ rpm, T = 25°C. a) The current densities are normalized to the ECSA of each electrocatalysts, b) The current densities are normalized to the electrode's active geometric surface area (i.e. 0.196 cm^2).

When looking closely at the CVs (Fig. 3a), especially in the potential range from $E = 0$ V to 0.30 V vs. RHE, the BOR kinetics are similar for the Pt/C-only electrode and the graded Pd/C|Pt/C electrode, but the BOR kinetics are faster on the mixed electrode and the graded Pt/C|Pd/C electrodes. These results indicate that, for the graded electrodes, the position of the electrocatalyst influences the resulting BOR kinetics. The ions/fuel diffusion through the catalytic layer may explain these observations: the electrocatalyst closest to the glassy carbon support, at the bottom of the catalytic layer, should have much poorer ions/fuel diffusion through the catalytic layer, so its characteristics will likely be less apparent in the CVs. Because Pt/C is active for the HOR, the Pd/C|Pt/C graded electrode (that has the Pd/C layer in direct contact with the electrolyte), yields lower apparent BOR kinetics, owing to (i) the smaller kinetics of BOR (and of HOR) at Pd/C than at Pt/C and (ii) the fact that most H_2 produced at the electrode surface does not reach Pt/C, and can be evacuated (because of the revolution rate of the RDE) prior to reaching any Pt/C site, that are all located in the inner layer of the graded thin-film (i.e. not in direct contact with the electrolyte).

In addition, the theoretical limiting current density that should be obtained in the conditions of the study was calculated using the Levich equation (Eq. 7):

$$j_{lim} = 0.62\, n\, F D^{\frac{2}{3}}\, \nu^{\frac{-1}{6}}\, C_0\, \omega^{\frac{1}{2}} \qquad [7]$$

where n is the number of electrons involved in the reaction, F is the Faraday's constant (A s mol^{-1}), D is the diffusion coefficient of the reactant (cm^2 s^{-1}), ν is the kinematic viscosity of the electrolyte (cm^2 s^{-1}), C_0 the reactant concentration (mol cm^{-3}) and ω is the working electrode rotation rate (rad s^{-1}).

The theoretical limiting current was calculated assuming that $n = 8e-$, $D = 3.01 \times 10^{-5}$ cm^2 s^{-1}, and $\nu = 0.0114$ cm^2 s^{-1} for $\omega = 167.55$ rad s^{-1}. The values of D and ν come from the study of Chatenet et al. for experimental conditions that most closely correspond to those of this work.[30] The theoretical limiting current density value was calculated to be 185 mA cm_{geom}^{-2} and is highlighted in Fig. 3b by the dashed red line. One can see that no clear

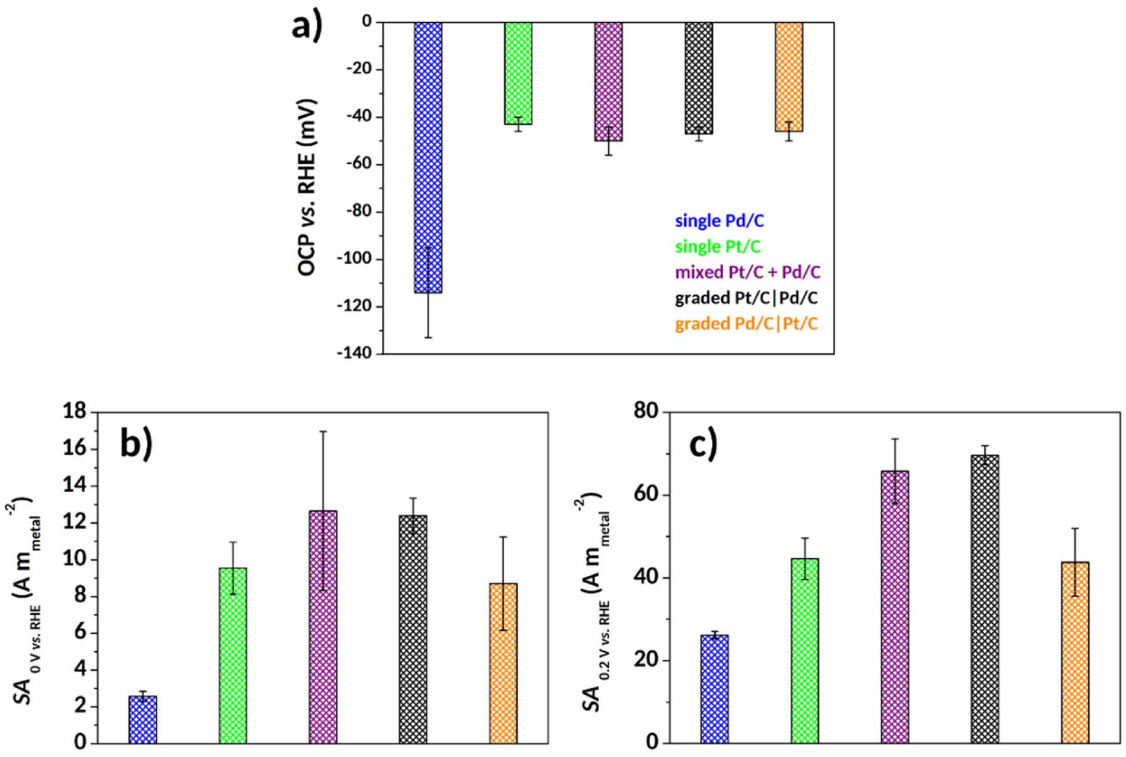

Figure 4. BOR activity markers: a) Open-circuit potential (OCP) values and specific activities (SA) at b) 0 V vs. RHE and c) 0.20 V vs. RHE measured from Figure 3.

limiting current densities appear on the BOR voltammograms obtained with each electrode configuration (Fig. 3b); thus, the theoretical limiting current density is compared to the maximum current density obtained (around $E = 0.80$ V vs. RHE) with each electrode configuration, which is 90, 83, 80, 80 and 70 mA cm_{geom}^{-2} for the Pd/C-only, Pt/C-only, mixed, graded Pt/C|Pd/C and graded Pd/C|Pt/C electrodes, respectively. These values are well below the theoretical limiting current density value calculated above, indicating that the 8 electrons are not reached. This observation is not surprising, assuming the small electrocatalyst loading (hence the small thickness of active layer) used here (i.e. 20 μg_{metal} cm^{-2}).[6]

The BOR activity was further analyzed by extracting the specific activity (SA) obtained at $E = 0$ and 0.20 V vs. RHE; the results are given in Figure 4a and Figure 4b, respectively. Even if Pd is able to start the BOR at a lower potential than Pt, the SA obtained with the Pd/C-only electrode at low potentials (and low $NaBH_4$ concentration) are significantly lower (4 to 6-fold lower at $E = 0$ V vs. RHE and 2 to 3-fold lower at $E = 0.20$ V vs. RHE) than for the Pt-containing electrodes, owing to the fast HOR kinetics on Pt. However, Figure 3a shows that the SA obtained on the Pd/C-only electrode is far greater than the SA obtained with the other electrode configurations beyond $E = 0.30$ V vs. RHE because at this potential, Pt sites are poisoned by BH_{ads} (and possibly $BH_{3,ads}$ species)[3,5] and Pt can therefore not completely oxidize the hydrogen species produced during the BOR.

The SA obtained with the graded Pt/C|Pd/C and mixed electrodes are nearly identical (see Figs. 4b and 4c) but higher than the SA obtained on Pd/C-only and Pt/C-only electrodes at low potential values (for $E < 0.20$ V vs. RHE, which is the practically relevant region for operation in a DBFC anode). However, when Pd/C is layered on top of the Pt/C, the SA is similar to that of the Pt/C-only electrodes. This result indicates that the position of the electrocatalyst in a graded electrode strongly influences the resulting BOR activity: an increase of ca. 30% of the SA is obtained with the graded Pt/C|Pd/C electrode, in comparison to the graded Pd/C|Pt/C electrode. In addition, the SA of the mixed electrode is not an average of the SAs of the Pt/C-only and Pd/C-only electrodes, showing a good synergy between the two materials when they are in close contact. We conclude that Pt and Pd in the mixed or graded electrode structures lead to improved BOR activity (in terms of low-potential kinetics) due to cooperative electrocatalysis.

H_2O_2-DBFC configuration measurement.—The impact of mixing or grading the electrocatalysts in the anodes of H_2O_2-DBFCs is further elucidated from the full-cell polarization and power curves using 0.01 M $NaBH_4$ (Figs. 5a, 5b) and 0.10 M $NaBH_4$ (Figs. 5c, 5d) at a cell temperature of $T = 25°C$. The net voltage at each current density is the sum of the cathode and anode losses from the theoretical cell voltage, so the cell voltage drops as the current density at the anode increases. While overpotentials in the anode and cathode activity result in a drop of the cell voltage, we assume that because of the use of a high surface area Pt/C electrode for H_2O_2 reduction (a fast reaction), the cells are not cathode-limited and the response is mainly due to the anode (however, because the polarization and power curves show the performance of the complete H_2O_2-DBFC, they may include some losses from the reduction of H_2O_2 at the cathode, especially at low

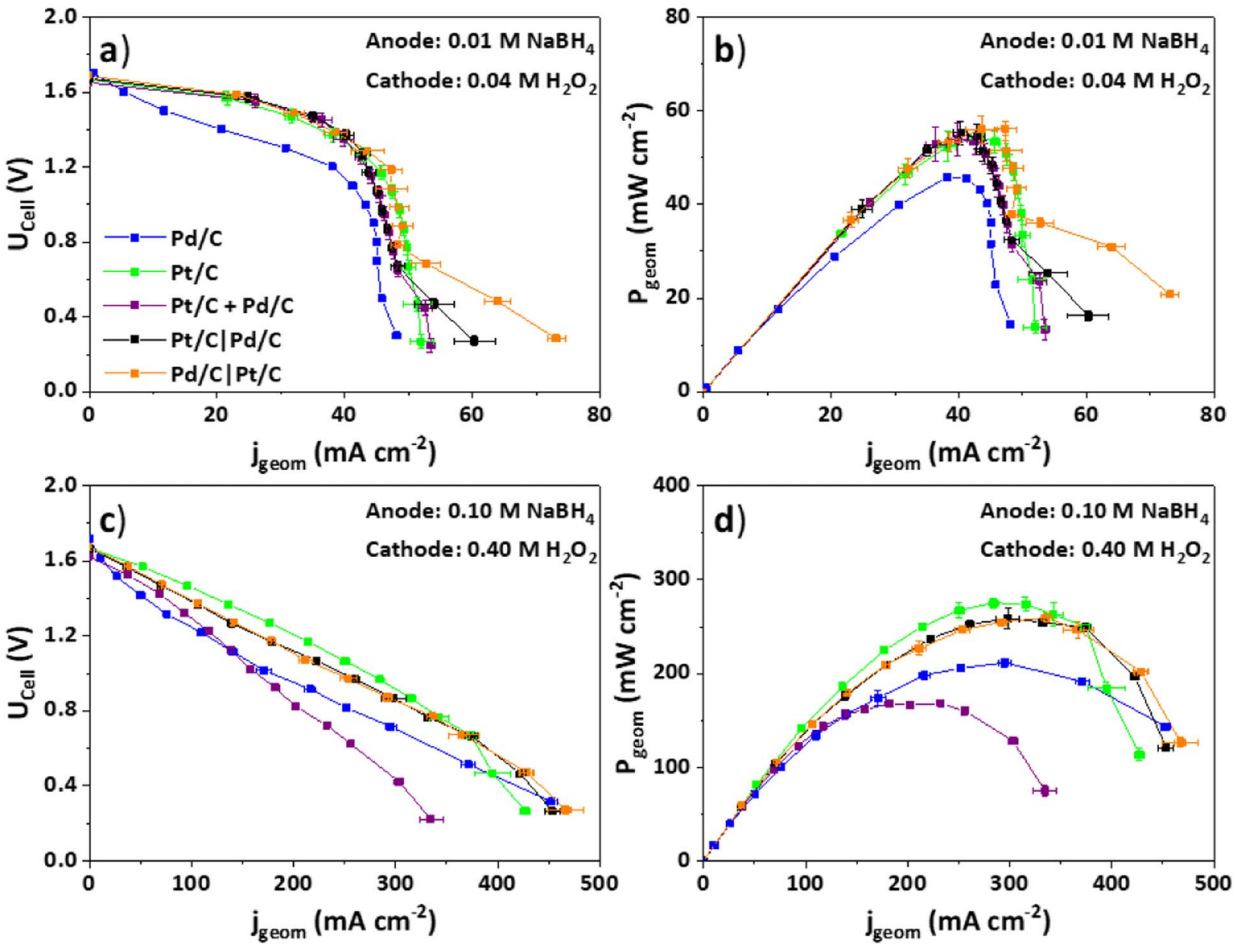

Figure 5. Electrochemical results for H_2O_2-DBFCs at 25°C: a) cell voltage vs. current density and b) power density vs. current density with 0.01 M $NaBH_4$ in 1 M NaOH fuel at the anode and 0.04 M H_2O_2 in 1 M H_2SO_4 electrolyte at the cathode; and c) cell voltage vs. current density and d) power density vs. current density using 0.10 M $NaBH_4$ in 1 M NaOH electrolyte at the anode and 0.40 M H_2O_2 in 1 M H_2SO_4 electrolyte at the cathode.

Table III. OCP values of the H_2O_2-DBFCs with Pd/C, Pt/C, Pt/C+Pd/C, Pt/C|Pd/C, and Pd/C|Pt/C anodes in 0.01 M and 0.10 M $NaBH_4$.

	OCV (V)				
[$NaBH_4$] (M)	Pd/C	Pt/C	Pt/C + Pd/C	Pt/C|Pd/C	Pd/C|Pt/C
0.01	1.70 ± 0.01	1.67 ± 0.01	1.65 ± 0.02	1.67 ± 0.01	1.67 ± 0.01
0.10	1.72 ± 0.02	1.67 ± 0.01	1.63 ± 0.02	1.67 ± 0.01	1.67 ± 0.02

cell voltage/high cell current). Table III shows the open circuit voltage (OCV) values obtained for each of the five anode configurations.

The electrochemical performance is drastically different between H_2O_2-DBFCs using Pd/C-only and Pt/C-containing anodes. At low $NaBH_4$ concentrations (Figures 5a, 5b), the H_2O_2-DBFCs using Pt/C-only, graded and mixed anodes have similar polarization curves, specifically performance at high cell voltages (U_{Cell} >1.30 V). H_2O_2-DBFCs with Pd/C-only anodes show much lower current density at all cell potentials, a slightly higher OCV (1.70 V) and different polarization curve behavior from the H_2O_2-DBFCs with Pt-containing anodes, suggesting a different BOR mechanism. As the cell voltage decreases, H_2O_2-DBFCs with Pt/C-containing anodes show a slight variance in performance from each other but in general maintain the same electrochemical behavior until $U_{Cell} \approx 0.80$ V. H_2O_2-DBFCs with graded Pd/C|Pt/C and mixed anodes have the highest geometric power density of 56.1 ± 0.6 and 54 ± 1 mW cm^{-2}, respectively. Those with Pd/C-only anodes only reach a power density of 45.7 ± 0.5 mW cm^{-2}. H_2O_2-DBFCs with Pt/C-only and graded Pd/C|Pt/C anodes have higher limiting currents as the cell voltage decreases (and the current density at the anode increases), reaching 47 ± 1 mA cm^{-2} at U_{Cell} = 1.20 V compared to 44 ± 2 mA cm^{-2} for those with mixed and graded Pt/C|Pd/C anodes. This corresponds to a value well below the expected limiting current density of 530 mA cm^{-2}. At cell voltages near 0.80 V, the fall-off in cell potential with increasing current density starts to plateau. The new plateau is observed with all five of the H_2O_2-DBFCs anodes, but is most pronounced in H_2O_2-DBFC with graded Pd/C|Pt/C anodes, and to a lesser extent in those with graded Pt/C|Pd/C anodes.

When the $NaBH_4$ concentration is increased to 0.10 M (Figures 5c, 5d), the H_2O_2-DBFCs with Pt/C-only anodes outperform the other four electrode configurations between OCV and 0.80 V. At 0.80 V, the cell has a current density of 350 mA cm^{-2}. This current density far exceeds the performance of similar cells in similar conditions,[7,31] for which the current density is approximately 18 mA cm^{-2}, presumably due to the use of a high surface area cathode. H_2O_2-DBFCs with the two graded anodes show equivalent performance to each other and only slightly smaller current densities than those with the Pt/C-only anodes, regardless of which electrocatalyst is placed closest to the fuel inlet. H_2O_2-DBFCs with mixed anodes only show higher current densities than those with Pd/C-only anodes at U_{Cell} > 1.20 V. Below 1.2 V, the cells with Pt + Pd mixed anodes have significantly lower current densities than all other H_2O_2-DBFCs, including those with Pd/C-only anodes.

H_2O_2-DBFCs with Pd/C-only anodes have higher OCV than those with Pt/C-containing anodes by about 50 mV at both $NaBH_4$ concentrations (see Table III): 1.70 V is reported at low concentration and 1.72 V is reported at high concentration for the Pd/C-only anodes, compared to 1.67 V for H_2O_2-DBFCs with Pt/C-containing anodes (1.63 V for H_2O_2-DBFCs with mixed anodes). The depression of the OCV with Pt is likely due to the existence of a mixed potential at the Pt surface due to the presence of H_2 gas along with BH_4^-.

Assuming that only the BOR occurs in the H_2O_2-DBFCs, the fuel utilization values are between 9.4% and 8.5% at the maximum current measured in the cell for low and high $NaBH_4$ concentrations respectively. The low fuel utilization can be attributed to the purposeful laminar flow in the cell design,[7] resulting in a lack of mixing. These values are far higher than what would be achieved in the RDE configuration used here, but well below desirable levels for a practical H_2O_2-DBFC. However, for the purpose of this work, the low fuel utilization is understood and consistent between cells.

The *H_2 escape* measurements are plotted vs. current density in Figure 6 for the five anode configurations. The *H_2 escape* results from the chemical heterogeneous hydrolysis of BH_4^- and BOR intermediates or of electrochemical reduction of water (at low anode potential/high cell voltage), followed by the resulting H_2 gas leaving the anode without being oxidized by the electrocatalyst.

At low $NaBH_4$ concentrations (see Fig. 6a), all Pt-containing anodes show similar *H_2 escape* trends. Each start with a relatively high value at current densities of 0 mA cm^{-2} (i.e. when U_{Cell} = OCV): mixed and both graded anodes have comparable *H_2 escape* to the Pt/C-only anodes (8 μL s^{-1}). As the current density increases (and U_{Cell} decreases), the *H_2 escape* for each Pt/C-containing anode decreases rapidly, approaching zero between 30 and 45 mA cm^{-2} (corresponding to U_{Cell} of 1.50 V and 1.30 V, respectively). Pd/C-only anodes have the lowest *H_2 escape* at OCV, with only 1.8 μL s^{-1} and have a gradual decrease in *H_2 escape* with increasing current density, but eventually approach a value close to zero at the comparable current density but much lower cell voltage compared to Pt/C-containing anodes. The *H_2 escape* increases slightly for the Pt/C-only and Pd/C-only anodes when the current density exceeds 45 mA cm^{-2} while it remains near zero for the mixed and both graded anodes. These trends overall are expected and match recent differential electrochemical mass spectrometry data obtained for Pt and Pd electrodes for low $NaBH_4$ concentration electrolytes (5 mM).[3,10]

With $NaBH_4$ concentrations of 0.10 M (see Figs. 6a, 6b), the *H_2 escape* trends become more distinct for the five anodes, with the Pd/C-only showing the opposite trend of the four Pt/C-containing anodes. The *H_2 escape* of the Pd-only anode at the OCV is low (2 μL s^{-1}) and exceeds 80 μL s^{-1} as the current density increases to 400 mA cm^{-2} ($U_{Cell} \approx 0.40$ V). This effect has also been observed by Braesch et al. and was accounted for by the inability of Pd to completely oxidize H_2 coupled to its larger $BH_{x,ads}$ poisoning at large borohydride concentration.[10] The Pt/C-only and mixed anodes show a similar trend as with the lower 0.01 M $NaBH_4$ concentration, where *H_2 escape* decreases with increasing current density, however, the decrease is more gradual presumably due to the higher BH_4^- to Pt ratio. Most striking is that the mixed anodes have approximately half the *H_2 escape* of Pt/C-only anodes at 0 mA cm^{-2} (28 μL s^{-1} for mixed anodes vs. 51 μL s^{-1} for Pt/C-only anodes). Mixed anodes also reach zero *H_2 escape* at a lower current density than Pt/C-only anodes. This shows that Pd/C decreases H_2 production and Pt oxidizes the H_2, hence showing the benefit of mixed electrodes.

Both the Pt to Pd and Pd to Pt graded anodes have a relatively constant *H_2 escape* regardless of the current density, between about 50 and 300 mA cm^{-2}. Above 300 mA cm^{-2}, the *H_2 escape* of graded Pt/C|Pd/C anode decreases. The decrease in *H_2 escape* corresponds to the U_{Cell} where there is a slight difference in behavior observed between graded Pt/C|Pd/C and Pt/C|Pd/C in the polarization curves (see Figure 5).

Figure 7 summarizes the results for current density, power density and *H_2 escape* in Figs. 5 and 6 for cell voltages of 1.40 V and 0.80 V in both 0.01 M and 0.10 M $NaBH_4$. We also include the numerical average (Avg) of the results for the Pt/C and Pd/C anodes as Avg (Pt/C and Pd/C) to determine whether there is any additive effect of the mixed or graded electrocatalysts. The results show variable results with cell voltage and $NaBH_4$, with different anodes performing best at different conditions. Overall, the Pt-only anodes have superior current density and power density. The mixed or graded anodes have comparable performance to the Pt-only anodes despite having only half the Pt, suggesting an active role of the Pd. A clear benefit of the mixed and

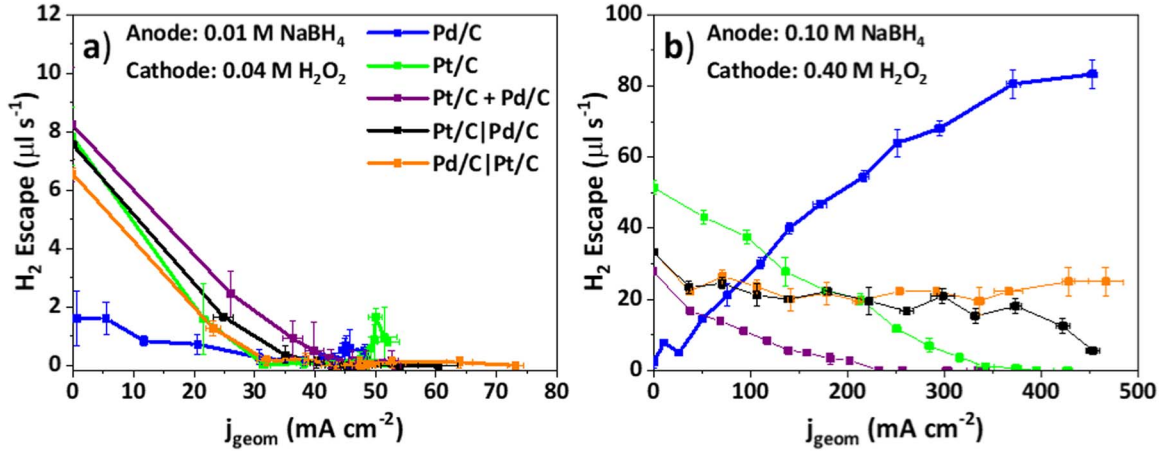

Figure 6. *H_2 escape* vs. current density at each H_2O_2-DBFC anode configuration a) in 0.01 M $NaBH_4$ + 1 M NaOH electrolyte at the anode and 0.04 M H_2O_2 + 1 M H_2SO_4 electrolyte at the cathode and b) in 0.10 M $NaBH_4$ + 1 M NaOH electrolyte at the anode and 0.40 M H_2O_2 + 1 M H_2SO_4 electrolyte at the cathode.

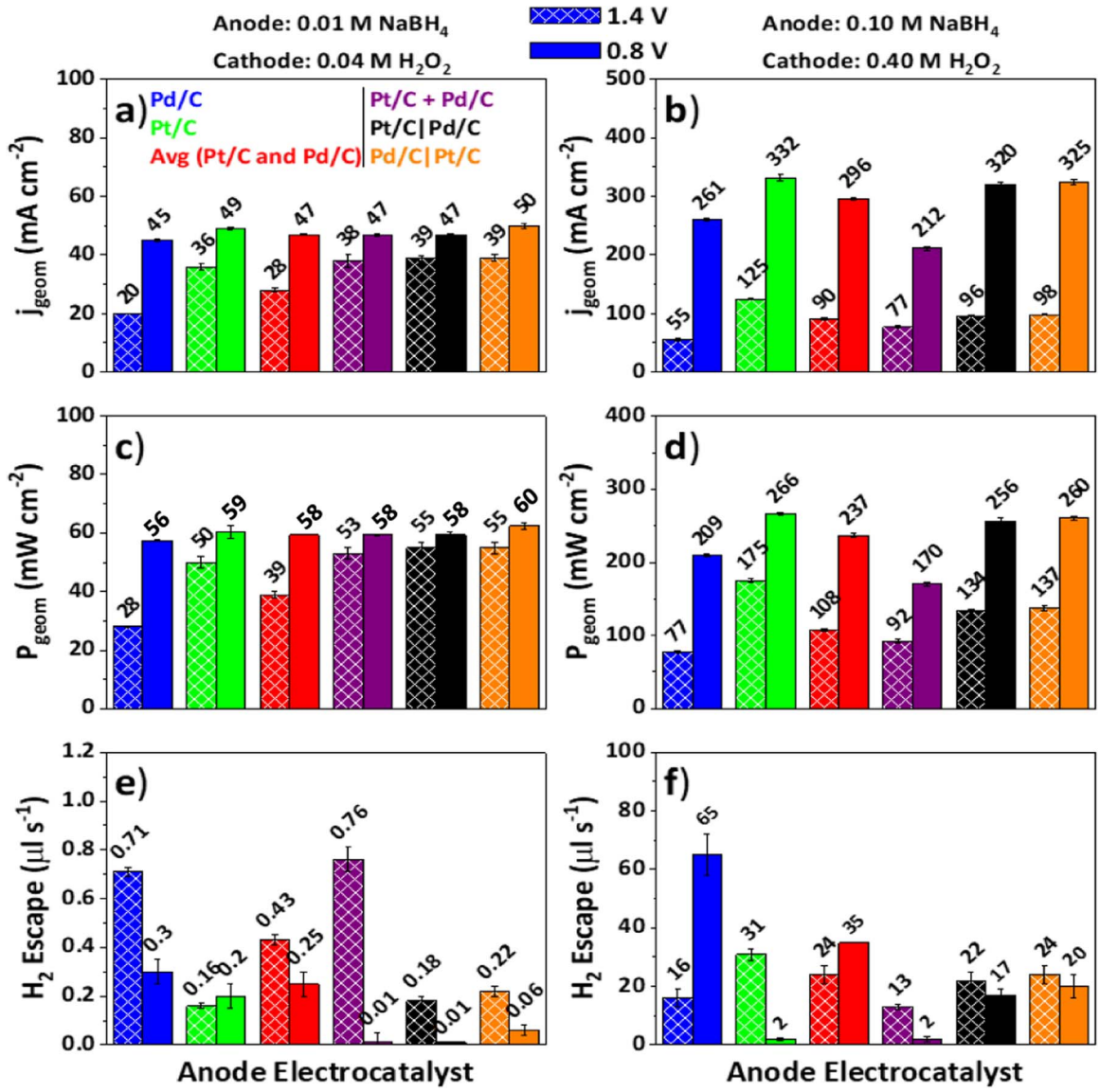

Figure 7. Summary of electrochemical analysis and H_2 escape for H_2O_2-DBFCs at cell voltages of 1.20 V (crisscross) and 0.80 V (solid): a) j_{geom} using 0.01 M $NaBH_4$, b) j_{geom} using 0.10 M $NaBH_4$, c) P_{geom} using 0.01 M $NaBH_4$, d) P_{geom} using 0.10 M $NaBH_4$, e) *H_2 escape* using 0.01 M $NaBH_4$ and f) *H_2 escape* using 0.10 M $NaBH_4$.

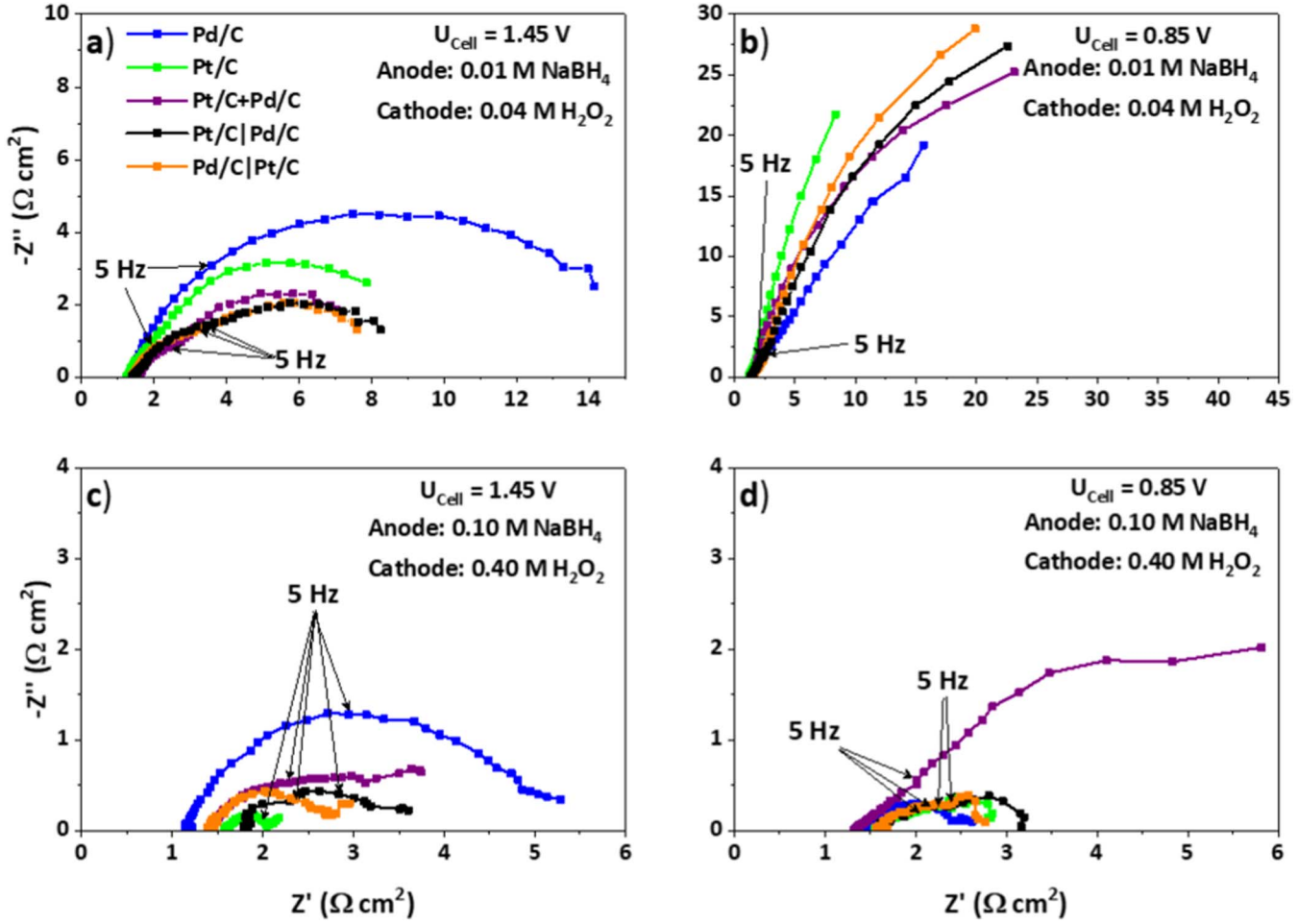

Figure 8. EIS plots of Pd/C (blue), Pt/C (green), mixed Pt/C+Pd/C (purple), graded Pt/C|Pd/C (black), and graded Pd/C|Pt/C (orange): a) Z' vs. $-Z''$ at $U_{Cell} \approx$ 1.45 V and b) Z' vs. $-Z''$ at $U_{Cell} \approx 0.85$ V using 0.01 M $NaBH_4$ in 1 M NaOH electrolyte at the anode and 0.04 M H_2O_2 in 1 M H_2SO_4 electrolyte at the cathode. c) Z' vs. $-Z''$ at $U_{Cell} \approx 1.45$ V and d) Z' vs. $-Z''$ at $U_{Cell} \approx 0.85$ V using 0.10 M $NaBH_4$ in 1 M NaOH electrolyte at the anode and 0.40 M H_2O_2 in 1 M H_2SO_4 electrolyte at the cathode.

graded electrodes is apparent in the *H_2 escape*, where the Pd decreases the *H_2 escape* when it is mixed with Pt, again suggesting that Pt and Pd serve as cooperative electrocatalysts.

Electrochemical impedance spectroscopy.—Select EIS results are shown in Figure 8 for H_2O_2-H_2O_2-DBFCs polarized to 200 mV ($U_{Cell} \approx 1.45$ V) and 800 mV ($U_{Cell} \approx 0.85$ V) at $NaBH_4$ concentrations of 0.01 M (Figures 8a, 8b) and 0.10 M (Figures 8c, 8d). These cell voltages correspond to conditions under which charge-transfer or mass-transfer limitations dominate the polarization curves (see Figure 5). Points at $\nu = 5$ Hz are indicated to show the general area where low frequency begins. The low frequency region ($10\ \text{Hz} < \nu < 0.1$ Hz) is mostly attributed to mass-transfer limitation, for which the mass-transfer resistance (R_{mt}) can be determined.[32] R_{mt} refers to the diffusion of reactants to and from corresponding catalyst layers and active electrocatalytic sites at both the anode and cathode. The total resistance and impedance in the high to moderate frequency range ($10^4\ \text{Hz} < \nu < 10$ Hz) is attributed to the resistance through the liquid electrolyte media and the membrane separator (Ohmic resistance, R_Ω), charge-transfer resistance through collector plates, anodes and electrocatalyst layers at both the anode and cathode (R_{ct}), and capacitance (Z_{CPE}) of the system.

The results show predominantly low frequency impedance responses in all H_2O_2-DBFCs using $NaBH_4$ concentrations of 0.01 M and H_2O_2 concentrations of 0.04 M for each cell voltage (Figs. 8a, 8b). When each H_2O_2-DBFC is polarized to 0.85 V (Fig. 8b), the impedance in the low frequency region ($\nu < 5$ Hz) increases. H_2O_2-DBFCs with Pt/C-only anodes have the highest impedance in the low frequency region, and those with Pd/C-only anodes have the lowest amplitude at $U_{Cell} \approx 1.24$ V. These increases directly correspond to the limiting current densities observed in the polarization results (see Figure 5a). Assuming that the cell is not cathode limited, the dominance of R_{mt} over R_{ct} is expected because of the low availability of reactants to catalyst active sites (the concentration of fuel was deliberately kept low in the study, this being especially true for 0.01 M $NaBH_4$).

The cell resistances decrease as the fuel concentration is increased to 0.10 M $NaBH_4$ and the oxidizer concentration increased to 0.40 M H_2O_2 (Figs. 8c, 8d), showing that the low frequency impedance and resistance are no longer dominant or no longer mass-transport limited by the low amount of reactant. Total resistances of each cell do not increase with low cell potential, with the exception of the H_2O_2-DBFCs with mixed anodes, which show a large increase in low frequency impedance and resistance. The results here are consistent with the polarization curves shown in Figure 6c, where H_2O_2-DBFCs using the mixed anodes reach lower current densities and geometric power densities than all other H_2O_2-DBFCs. The reason for this is discussed later.

The Ohmic resistance of H_2O_2-DBFCs with 0.10 M $NaBH_4$ fuel increases after the cell is polarized. In the H_2O_2-DBFCs with Pt-containing anodes, R_Ω is lower at high cell polarizations (800 mV). These trends are not observed in cells using $NaBH_4$ concentrations of 0.01 M. For example, at the OCV of H_2O_2-DBFCs using Pt/C-only anodes, R_Ω is 1.06 Ω cm^2 and increases to 1.65 Ω cm^2 at 600 mV

polarization (Table S1). It then decreases to 1.55 Ω cm^2 at 800 mV cell polarization. R_Ω from H_2O_2-DBFCs with Pd/C-only anodes continue to increase from 1.06 Ω cm^2 to 1.41 Ω cm^2 between 1.45 V and 0.85 V. A likely cause of this is the formation of H_2 bubbles within the active layer (and hence in the liquid electrolyte), that mask the active sites at the anode and hinder the ionic current flow. Other possible causes are a formation of a double layer increasing resistance to the cathode surface and insulation of the layer by BO_2^- "gel" (this phenomenon has been detected in in situ FTIR experiments.[32]

Discussion

Graded catalyst layers of Pt/C and Pd/C and their mixtures have in some cases an improvement in the BOR efficiency and H_2O_2-DBFC performance, mostly via a decrease of their H_2 escape, and in other cases result in no effect. A number of limiting factors may affect the performance of the H_2O_2-DBFCs, including an incomplete BOR regardless of catalyst or $NaBH_4$ concentration used. These limitations are evident from the low fuel utilization (Table S2) and the current densities obtained from all H_2O_2-DBFCs compared to the calculated limiting current density values (0.53 A cm^{-2} and 5.30 A cm^{-2} for 0.01 M and 0.10 M $NaBH_4$, respectively). The current limitations at stake include:

1) Too-slow BOR and HOR kinetics at the Pt and Pd electrocatalysts;
2) Surface poisoning of the catalysts, especially at higher $NaBH_4$ concentrations;
3) Hindrance by H_2 bubbles blocking active surfaces keeping reaction species from being oxidized;
4) Mass-transport or Ohmic limitations due to cell design, reactant concentrations, and the Nafion 117 membrane;
5) Cathode limitations at lower cell voltage.

At the lower $NaBH_4$ concentrations, Pt dominates the apparent BOR and HOR current at all Pt-containing electrodes as can be seen from the RDE configurations. From the H_2O_2-DBFCs with Pt-containing anodes, we also see little difference between each polarization curve and *H_2 escape* measurements. In each case, the curves resemble that of H_2O_2-DBFCs with Pt/C-only anodes and differ from those with Pd/C-only anodes. However, it is difficult to ascertain kinetic properties at these concentrations within the H_2O_2-DBFCs because they are mass-transfer limited. This is apparent from the EIS results (Figures 8a, 8b), where the low frequency impedance is significant at $U_{Cell} \approx 0.85$ V. The mass-transfer impedance is an artifact of both the cell design[31] as well as the low availability of reaction species for electrooxidation and diffusion. Poisoning as a limitation is less of an issue at the lower concentration, because there is a high ratio of available active surface area to available BH_4^-. The electrocatalysts can therefore accommodate BH_4^-, BOR reaction intermediates, H_2 and H_{ads} oxidation when the half-cell potential exceeds 0 V vs. RHE, and this accounts for the minimal *H_2 escape* (see Figure 6) and low current density.

The overall performance of the graded anodes differ using RDE versus the H_2O_2-DBFC. Using the RDE configuration, the graded Pt/C|Pd/C anode outperforms the graded Pd/C|Pt/C one at both half-cell potentials of 0 and 0.20 V vs. RHE (corresponding to approximate (full) cell voltages of 1.65 V and 1.45 V, respectively). This is not the case using the H_2O_2-DBFC, in which there is little difference in performance between cells with graded anodes at most cell voltages. Pd/C|Pt/C anodes lead to higher current densities than Pt/C|Pd/C anode at higher loads. These differences can be attributed to differences in catalyst layer composition and cell design. The RDE has layers graded one on top of the other while the H_2O_2-DBFC has layers graded along the flow field from inlet to outlet. In the RDE, the second electrocatalyst type added to the graded electrode is closer to the convection boundary layer than the first. Alternatively, in the H_2O_2-DBFC electrode, each catalyst type has similar boundary layer thickness, but may be exposed to different concentrations of ions in the fuel depending on which type of catalyst is upstream. Each catalyst in the H_2O_2-DBFC is on one wall of a laminar flow field (Figures 1 and 2), allowing some reactants to flow through the cell without interacting with the catalyst, so some BH_4^- flows through that is unreacted. Additionally, the RDEs are more likely kinetically controlled, at least at low potential (owing to the lower catalyst area loading), whereas the H_2O_2-DBFCs are more likely mass-transfer limited at the lower concentrations. The cathode might also be limiting the H_2O_2-DBFC performance in some of the cells.

More variation in performance is measured between each H_2O_2-DBFC with Pt-containing anodes when the $NaBH_4$ concentration is increased to 0.10 M. The Pd appears to play a more substantial role in the performance especially in H_2O_2-DBFCs with mixed anodes. This is evident from changes in polarization curve shape and *H_2 escape* from the anode. Surface poisoning of the Pt and Pd by intermediate adsorbate species, bubble formation, double layer formation, as well as other causes of R_Ω and R_{mt} are also contributing factors.

To understand the role of Pd in the overall cell performance and as a cooperative catalyst with Pt, several factors including the production and escape of un-oxidized gaseous H_2 are considered. A previous study using Pd have shown reduced H_2 production at Pd when compared to Pt.[10] Pd electrodes produce H_2 at OCV due to the chemical heterogeneous hydrolysis of BH_4^- to BH_3OH (and HER, to some extent) in these studies; however, the results in Figure 7 show minimal *H_2 escape* prior to current flow at both $NaBH_4$ concentrations used and significant increases when current is flowing at $NaBH_4$ concentrations of 0.10 M. The authors speculate that while there is some chemical H_2 generation at Pd at OCV when a load is applied, partial electrooxidation of BH_4^- to BH_3-like intermediates (Eq. 8) followed by the hydrolysis of $BH_{3,ads}$ to $H_2 + BH_{ads}$ (Eq. 9) proceed.

$$BH_4^- \rightarrow BH_{3,ads} + H^+ + 2\,e^- \quad [8]$$

$$BH_{3,ads} \rightarrow BH_{ads} + H_2 \quad [9]$$

The long reactant residence times, and/or poisoning by adsorbate species on the Pd, prevent significant oxidation of H_2, leading to an elevation of *H_2 escape* from the anode.[10] Additionally, a contributing factor is slow HOR kinetics on Pd in alkaline media.[33]

The BH_{ads} produced from Eq. 9 may undergo further hydrolysis producing more *H_2 escape* or oxidation to BO_2^- giving a 4-electron BOR reaction instead of a complete 8-electron reaction. This is supported by observations seen by Grimmer et al. using RRDE to evaluate the behavior of Pd for BOR shown in Eq. 10, although in their paper, they propose BH_2 species as the intermediate at stake in the 4-electron BOR (but in their case, they relied on rotating ring-disk experiments with a Pt-ring to detect reaction intermediates, which is not wise as Pt is active for the oxidation of BH_4^-, all its intermediates and H_2, hence is not (at all) selective).[12] The initially lower *H_2 escape* observed from Pd-only anodes at the higher $NaBH_4$ concentrations (see Fig. 6b) and inflection seen in the polarization curves (see Fig. 5c) as U_{Cell} decreases ($U_{Cell} < 0.80$ V) may be indicative of a shift in the BOR mechanism or improved HOR. It is however evident given these cell conditions, that Pd is not an effective catalyst for a full 8-electron BOR when used alone, in particular at high $NaBH_4$ concentrations, in line with Olu et al.[9] and Braesch et al. earlier reports.[10]

$$BH_4^- + 4\,OH^- \rightarrow BO_2^- + 2\,H_2O + 2\,H_2 + 4\,e^- \quad [10]$$

A significant difference in *H_2 escape* is observed between H_2O_2-DBFCs with Pt-containing anodes and Pd/C-only anodes, especially when $NaBH_4$ concentrations are at 0.10 M. *H_2 escape* caused by hydrolysis of BH_4^- (and/or HER) at 0 mA cm^{-2} catalyzed at the Pd/C-only anode is minimal compared to Pt/C-only anodes. Therefore, it can be concluded that most H_2 production and subsequent escape are the result of BH_4^- hydrolysis (and/or HER) by the Pt in the mixed and graded anodes of the H_2O_2-DBFC. As the current is increased, the source of *H_2 escape* begins to shift from H_2 produced at the Pt, to H_2 being produced at Pd (see Fig. 6b).

Using the above assumptions, we posit that at graded Pd/C|Pt/C anodes, the BH_4^- may be oxidized first by Pd (this agrees with the lower OCVs of DBFCs with Pd vs Pt anodes) and the resulting $BH_{3,ads}$

may be further oxidized by Pt to BH_{ads} (Eq. 11).

$$BH_{3,ads} + 2\,OH^- \rightarrow BH_{ads} + 2\,H_2O + 2\,e^- \quad [11]$$

The lower *H_2 escape* measured when the current density exceeds 350 mA cm^{-2} from the graded Pt/C|Pd/C anode (see Fig. 6b), which is not seen from the Pd/C|Pt/C anode, is an indication of lower poisoning when Pt/C is located at the outlet. Pt poisoning at the inlet due to Pt oxide formation (at low cell voltage) or reaction adsorbate species combined with slower *H_2 escape* at Pd at lower cell voltage may explain why less *H_2 escape* is measured. This may also explain why there is a deviation in performance at the corresponding cell voltage, where Pt/C|Pd/C gives lower current densities and power densities (see Figs. 5c, 5d). At these concentrations, the active surface area is likely (at least partially) blocked by H_2 bubbles and/or poisoned from adsorbate species, especially in the H_2O_2-DBFC with mixed anodes.

The question remains why the H_2O_2-DBFC with the mixed anode performs so poorly compared to all others. This H_2O_2-DBFC anode configuration may be significantly limited by the amount of Pt on the surface, only seeing benefits from lower *H_2 escape* compared to each H_2O_2-DBFC with graded anodes that result in a higher current density, which is much closer to H_2O_2-DBFCs with Pt-only anodes. The low current densities accompanied by low *H_2 escape* indicate that poisoning by adsorbate species of both Pt and Pd lowers the available active sites for electrocatalysis. In addition, Pt is capable to oxidize the H_2 produced by Pd; in this scenario, Pd would react with incoming BH_4^- in priority, leading to $BH_{x,ad}$/Pd species and H_2, the latter being easily oxidized on the free surfaces of Pd because of the closer proximity to the Pt than at either of the graded anodes. The results from the EIS of the H_2O_2-DBFCs with mixed anode support the former conclusion. They show a large increase in the low frequency impedance/resistance (not seen in the other H_2O_2-DBFCs, see Fig. 8d), which is consistent with high levels of poisoning or slower reaction rates, overall causing increases in the mass-transfer resistance.

Summary

We demonstrate that Pt and Pd can act as cooperative electrocatalysts for the BOR under some conditions. Using half-cell RDE and full-cell H_2O_2-DBFC measurements in two different $NaBH_4$ concentrations, we showed that mixtures and gradients of Pt/C and Pd/C electrocatalysts have improved electrocatalytic performance and less deleterious *H_2 escape* when compared to cells having catalyst layers with Pt- or Pd-only.

The cooperative effect can be attributed to the different BOR characteristics for Pt and Pd. Pt is known to oxidize BH_4^- to $BH_{ads} + H_{ads}$, the latter of which can progress to unreacted H_2. The $BH_{3,ads}$ formed by Pd oxidation of BH_4^- can be desorbed into BH_3OH^- species and (easily) oxidized to BH_{ads} by Pt. Pt is also highly susceptible to BH_{ads} poisoning. Pd is prone to oxidize BH_4^- to $BH_{3,ads}$. When used with Pd, this study suggests that the BH_{ads}-poisoned Pt is effective at converting the Pd-generated BH_3-like species to BH_{ads}, but not BH_4^- directly to BH-like species. The low *H_2 escape* observed with the mixed and graded anodes compared to Pt/C-only anodes, especially at working cell conditions above $U_{Cell} = 1.45$ V, leads to the conclusion that the presence of Pd in an in-plane graded configuration with Pt is beneficial to the overall performance of a H_2O_2-DBFC, especially at high BH_4^- concentrations.

For future work, it is possible that other catalysts (aside from the Pd and Pt studied here) could provide superior BOR activity and subsequent DBFC performances in a graded electrode configuration. The cooperative effect between Pt and Pd may change when cell temperatures are increased to practical temperatures near $T = 60°C$ and the fuel utilization is improved. However, we can conclude that for complex reactions such as the BOR, more complex electrode architectures with multiple catalysts offer a promising approach.

Acknowledgments

NRL thanks the Office of Naval Research (ONR) for funding. LEPMI would like to thank ONR Global for support (grant number N62909-16-1-2137). Some of this work has been performed within the framework of the Centre of Excellence of Multifunctional Architectured Materials "CEMAM" n° ANR-10-LABX-44-01.

ORCID

Robert W. Atkinson III https://orcid.org/0000-0001-7575-0584
Yannick Garsany https://orcid.org/0000-0002-8943-7174
Marian Chatenet https://orcid.org/0000-0002-9673-4775
Karen Swider-Lyons https://orcid.org/0000-0001-5746-1949

References

1. M. Unlu, J. F. Zhou, and P. A. Kohl, *J. Phys. Chem. C*, **113**, 11416 (2009).
2. B. H. Liu, Z. P. Li, and S. Suda, *Electrochim. Acta*, **49**, 3097 (2004).
3. P. Y. Olu, A. Bonnefont, G. Braesch, V. Martin, E. R. Savinova, and M. Chatenet, *J. Power Sources*, **375**, 300 (2018).
4. Z. Jusys and R. J. Behm, *Electrochem. Commun.*, **60**, 9 (2015).
5. P. Y. Olu, A. Bonnefont, M. Rouhet, S. Bozdech, N. Job, M. Chatenet, and E. Savinova, *Electrochim. Acta*, **179**, 637 (2015).
6. K. S. Freitas, B. M. Concha, E. A. Ticianelli, and M. Chatenet, *Catal. Today*, **170**, 110 (2011).
7. R. O. Stroman and G. S. Jackson, *J. Power Sources*, **247**, 756 (2014).
8. J. Ma, N. A. Choudhury, and Y. Sahai, *Renew Sust Energ Rev*, **14**, 183 (2010).
9. P. Y. Olu, F. Deschamps, G. Caldarella, M. Chatenet, and N. Job, *J. Power Sources*, **297**, 492 (2015).
10. G. Braesch, A. Bonnefont, V. Martin, E. R. Savinova, and M. Chatenet, *Electrochim. Acta*, **273**, 483 (2018).
11. M. Simoes, S. Baranton, and C. Coutanceau, *J. Phys. Chem. C*, **113**, 13369 (2009).
12. C. Grimmer, M. Grandi, R. Zacharias, B. Cermenek, H. Weber, C. Morais, T. W. Napporn, S. Weinberger, A. Schenk, and V. Hacker, *Appl. Catal. B-Environ*, **180**, 614 (2016).
13. H. Y. Qin, K. J. Chen, C. Zhu, J. B. Liu, J. Wang, Y. He, H. Z. Chi, H. L. Ni, and Z. G. Ji, *J. Power Sources*, **299**, 241 (2015).
14. J. Q. Yang, B. H. Liu, and S. Wu, *J. Power Sources*, **194**, 824 (2009).
15. I. Merino-Jimenez, M. J. Janik, C. Ponce de Leon, and F. C. Walsh, *J. Power Sources*, **269**, 498 (2014).
16. M. G. Hosseini and R. Mahmoodi, *J. Power Sources*, **370**, 87 (2017).
17. V. L. Oliveira, E. Sibert, Y. Soldo-Olivier, E. A. Ticianelli, and M. Chatenet, *Electrochim. Acta*, **209**, 360 (2016).
18. V. L. Oliveira, E. Sibert, Y. Soldo-Olivier, E. A. Ticianelli, and M. Chatenet, *Electrochim. Acta*, **190**, 790 (2016).
19. R. M. E. Hjelm, Y. Garsany, R. W. Atkinson III, R. O. N. Stroman, K. Swider-Lyons, C. Lafforgue, and M. Chatenet, *ECS Trans*, **80**, 1033 (2017).
20. I. Katsounaros, W. B. Schneider, J. C. Meier, U. Benedikt, P. U. Biedermann, A. A. Auer, and K. J. J. Mayrhofer, *Phys. Chem. Chem. Phys*, **14**, 7384 (2012).
21. Y. L. Zheng, W. Chen, X. Q. Zuo, J. Cai, and Y. X. Chen, *Electrochem. Commun.*, **73**, 38 (2016).
22. R. W. Atkinson III, R. R. Unocic, K. A. Unocic, G. M. Veith, T. A. Zawodzinski, and A. B. Papandrew, *ACS Appl Mater Inter*, **7**, 10115 (2015).
23. A. B. Papandrew, C. R. I. Chisholm, R. A. Elgammal, M. M. Ozer, and S. K. Zecevic, *Chem. Mater.*, **23**, 1659 (2011).
24. S. St John, R. W. Atkinson III, R. R. Unocic, T. A. Zawodzinski, and A. B. Papandrew, *J. Phys. Chem. C*, **119**, 13481 (2015).
25. J. A. McCaulley, *Phys. Rev. B*, **47**, 4873 (1993).
26. S. B. Ziemecki, G. A. Jones, D. G. Swartzfager, and R. L. Harlow, *J. Am. Chem. Soc.*, **107**, 4547 (1985).
27. C. C. Herrmann, G. G. Perrault, and A. A. Pilla, *Anal. Chem.*, **40**, 1173 (1968).
28. Y. Garsany, I. L. Singer, and K. E. Swider-Lyons, *J. Electroanal. Chem.*, **662**, 396 (2011).
29. M. B. Sassin, Y. Garsany, B. D. Gould, and K. E. Swider-Lyons, *Anal. Chem.*, **89**, 511 (2017).
30. M. Chatenet, M. B. Molina-Concha, N. El-Kissi, G. Parrour, and J. P. Diard, *Electrochim. Acta*, **54**, 4426 (2009).
31. R. O. Stroman, G. S. Jackson, Y. Garsany, and K. Swider-Lyons, *J. Power Sources*, **271**, 421 (2014).
32. B. M. Concha, M. Chatenet, E. A. Ticianelli, and F. H. B. Lima, *J. Phys. Chem. C*, **115**, 12439 (2011).
33. J. Durst, A. Siebel, C. Simon, F. Hasné, J. Herranz, and H. A. Gasteiger, *Energ Environ Sci*, **7**, 2255 (2014).